AEROSOL SELF-ASSEMBLY OF NANOPARTICLE FILMS: GROWTH DYNAMICS AND RESULTING 3D STRUCTURE

Noushin Nasiri[a], Tobias D. Elmøe[b], Qinghua Qin[c], Antonio Tricoli[a,*]

[a] **Nanotechnology Research Laboratory, Research School of Engineering, College of Engineering and Computer Science, Australian National University**

[b] **Amminex Emissions Technology A/S, Gladsaxevej 363, 2860 Søborg, Denmark**

[c] **Research School of Engineering, College of Engineering and Computer Science, Australian National University**

ABSTRACT

In this study, aerosol deposition of nanoparticles on flat surfaces has been investigated by Langevin dynamics (LD) accounting for Brownian's diffusion and a fix translational velocity. The particles are assumed to drop one at a time and had a monodisperse size distribution. The detailed morphology of the nanoparticle films was investigated as a function of Pe number, the ratio between Brownian and translational displacement for different structural constrains. The porosity was reduced with increasing Pe number from the diffusion to ballistic deposition limit. It was found that the simulation constrains have a substantial impact on the resulting film structural properties. This was attributed to the multi-scale porosity of these aerosol-deposited films.

Keyword: Deposition, Nanoparticle, Porosity, Aerosol, Self-Assembly, Nanoparticles, Sensors.

INTRODUCTION

Highly porous films of nanoparticles have shown potential for several technologies such as batteries [1], dye sensitized solar cells (DSSCs) [2], sensors [3] and catalytic [4] applications. Recently, chemo-resistive gas sensors made of metal oxide semiconductors have been used as detectors in breath analysis [5]. The sensing properties of these sensors can be drastically improved by reducing their size to the nanoscale [6-8]. It has been reported that the sensitivity of SnO_2 sensors to 1000 ppm ethanol was triplicated by changing the grain size from 35 to 10 nm [9]. The sensing films can be categorized in to three groups: dense, compact and porous films [15]. High porous films are advantageous for gas sensors because the gas molecules can diffuse effortlessly into the detector and chemical interactions can easily occur between the gas and the sensor surface [100, 11]. Nanoparticle generated in aerosol reactors can be directly deposited on sensor substrates to rapidly produce uniform and highly porous films. Aerosol deposition leads typically to highly porous morphologies [11]. There are several possibilities to form nanoparticle films by aerosol deposition. Among others, a hot aerosol of nanoparticles produced by a flame reactor can deposit thermophoretically on a cooled substrate resulting in the rapid growth of highly porous films [12, 13].

Fourth International Conference on Smart Materials and Nanotechnology in Engineering, edited by Jayantha A. Epaarachchi, Alan Kin-tak Lau, Jinsong Leng, Proc. of SPIE Vol. 8793, 879320 · © 2013 SPIE · CCC code: 0277-786X/13/$18 · doi: 10.1117/12.2029520

Engineering of the sensor properties to produce highly performing devices requires an advanced understanding of multi-scale phenomena such as particle-, fluid- and molecule-dynamics. Here, modeling of the particle deposition dynamics is performed assuming spherical mono-disperse particle. The effect of different conditions on the film properties such as its porosity is investigated. Several works have been investigated the film assembly by controlling particle transports and chemical reactions [14]. Rodriguez et al [15] studied the simulation of particle deposition by an on-lattice Monte Carlo model over a planar flat surface. In 2006, Madler et all [11] reported the deposition of single and agglomerated particles based on the Langevin equation of motion. Agglomerate deposition of nanoparticles was able to generate films having higher porosities in comparison to the deposition of single spherical particles.

In this paper, the simulation of single particle deposition on a flat substrate has been investigated. The variables were the film thickness and Peclet number. The Pe number was varied from 10^{-7} to 100. The impact of these deposition parameters on the simulating of film morphology was investigated.

MODEL OUTLINE

The particles are assumed to move due to the Brownian motion and with respect to an external forces acting on the particle. The external force resultant is assumed to be constant in time for each simulation and is functional to the translational velocity towards the deposition surface. The particle movement is determined by using the Langevin equation of motion|:

$$mv = -f(v-w) + F + X \quad (1)$$

where m is the particle mass, v is the particle velocity, f is the friction factor, w is the fluid velocity, F is an external force and X is a random Brownian force. Change in translational velocity due to particle size and morphology is neglected. Interactions between particle-particle and particle-surface such as van der Waals and electrostatic forces are neglected. The particle deposition mechanism is controlled by the diffusion or translational velocity of the particle ranging from diffusion to the ballistic limit regime. The particles are assumed as monodisperse with a constant diameter of 50 nm and density of 1 g/cm^3 at 298 ºK. The particles are assumed to deposit one at the time. The first particle drops from a specific height, therefore it goes through an empty domain where no deposition is allowed and the particles reach a random distribution. The next particle is released after deposition of the previous one. Deposition happens when a particle touches another particle or the deposition surface.

RESULTS AND DISCUSSION

Figure 1 and 2 show the porosity of films made of single spherical particles (50 nm in diameter) as a function of their thickness with Peclet number (Pe) of 100 and 10^{-7}. The dimensionless Pe number is defined as following:

$$\mathrm{Pe} = \frac{(d_p/2)\ v}{D_p} \quad (2)$$

where d_p is the particle diameter, v is the velocity and D_p is particle diffusivity [11]. Therefore, the Pe number is the ratio of the definite particle motion to the indefinite particle random walk [15]. At small Pe, the particle transport is dominated by diffusion (diffusion limit) and very porous film is expected. In contrast, when the Pe number is larger than 1, the translational velocity is dominant (ballistic limit) leading to more compact films.

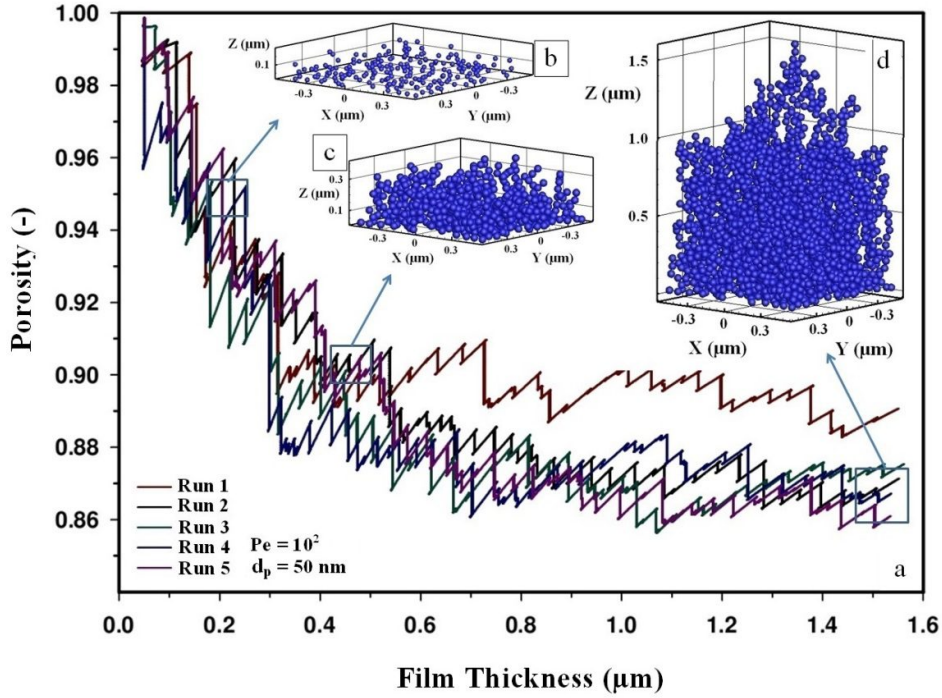

Figure 1: Film porosity for deposition of single spherical particles (50 nm in diameter) at a Pe of 100 as a function of the film thickness for 5 different simulations.

Figure 1 shows the film porosity as a function of film thickness for several simulations. There are strong variations in the simulated porosity in the initial stage of deposition. This is due to the small number of particles deposited (Fig. 1 insect b). In fact, at this stage if the particle deposits on the film surface or on a deposited particle, it changes drastically the particle deposition dynamics. Deposition on the top of the deposited particle leads to the growth of fractal-like branch structures that have low density. Upon deposition of 1 µm a considerable number of particles deposited on the surface resulting in a more reproducible morphology. At this stage, the total porosity and morphology will not change significantly as a function of deposition place of the particle. As a result at higher film thickness, the change in porosity is less sensible to fluctuations.

Figure 2 shows the same mechanism takes place at lower Pe number (10^{-7}). These results show that for all film thicknesses, the porosity of the film is higher for small Pe number than for large ones. It increases from 0.880 to 0.975 with Pe increasing from 100 to 10^{-7}. The 3D morphology of the films is shown in Figures 1 and 2 for several film thicknesses (0.2, 0.4 and 1.5 µm). They visualize further that the porosity of the deposited film decreases with increasing the number of deposited particle. Furthermore, this porosity is higher at smaller Pe numbers due to the particle deposition mechanism. The particle deposition morphology is tree-like at a Pe of 10^{-7} leading to higher porosity compared to bush-like deposition at a Pe of 100.

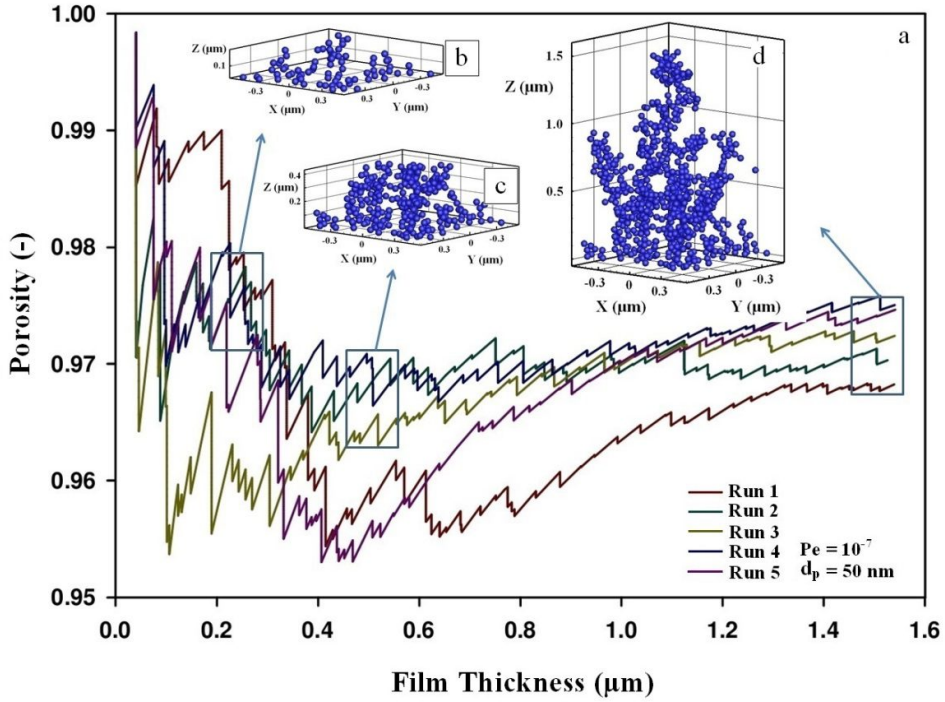

Figure 2: Film porosity for single spherical particles (50 nm in diameter) at a Pe of 10^{-7} as a function of the film thickness for 5 simulations.

At larger Pe number (Pe = 100), the number of deposited particles at given thickness is higher than at smaller Pe (Pe = 10^{-7}). In fact, at small Pe the particle transport is dominated by diffusion. For this case, the deposited film grows with the fractal-like structure. In contrast, when the Pe number is large, the translational velocity is dominant (Ballistic limit). In this regime, the particles have high translational velocity pile-up with more density. Therefore, more particles are required to be deposited to reach the same thickness in the ballistic limit than in the diffusion one. In the diffusion regime, particle displacement is dominated by Brownian diffusion and particles have nearly zero translational velocity. As a result, the composed film has tree-like structure with the highest possible porosity. For example, the number of deposited particles at a thickness of 0.2, 0.4 and 1.5 µm is 200, 650 and 2590 particles at a Pe of 100 and 75, 290 and 747 particles at a Pe of 10^{-7}.

Figure 3 shows the average film porosity for single spherical particles as a function of the thickness with increasing Pe numbers from 10^{-7} to 100. The porosity decreases with increasing the film thickness for all Pe numbers. These drops are accentuated in the beginning of the deposition and level-off at thickness higher that 1.2 µm. Moreover, at a constant thickness the porosity decreases by transition from diffusion to ballistic limit. However, the porosity variation is negligible with increasing Pe number from 10^{-7} to 10^{-2} (~0.975). While, the film porosity drops rapidly to 0.87 at Pe equals to 10. Increasing the Pe number to 100 results in the same porosity (0.87).

Figure 4 shows the three-dimensional nanoparticle network at a final thickness of 1.5 µm and Pe numbers of 10^{-7} to 100. These morphologies show the porosity variation during the transition from the diffusion to the ballistic limit. It can be seen that the deposition mechanism is tree-like for the Pe number ranging from 10^{-7} to 10^{-2}. However, at higher Pe number the deposition mechanism changes form tree-like to bush-like. Consequently, the number of deposited particles increases which leads to lower final porosity.

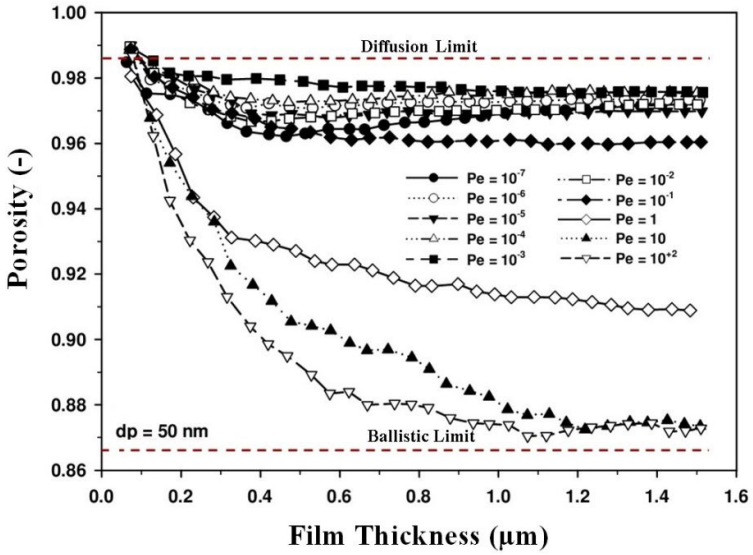

Figure 3: Average film porosity for single spherical particles (diameter of 50 nm) as a function of the thickness with increasing Pe numbers from 10^{-7} to 100.

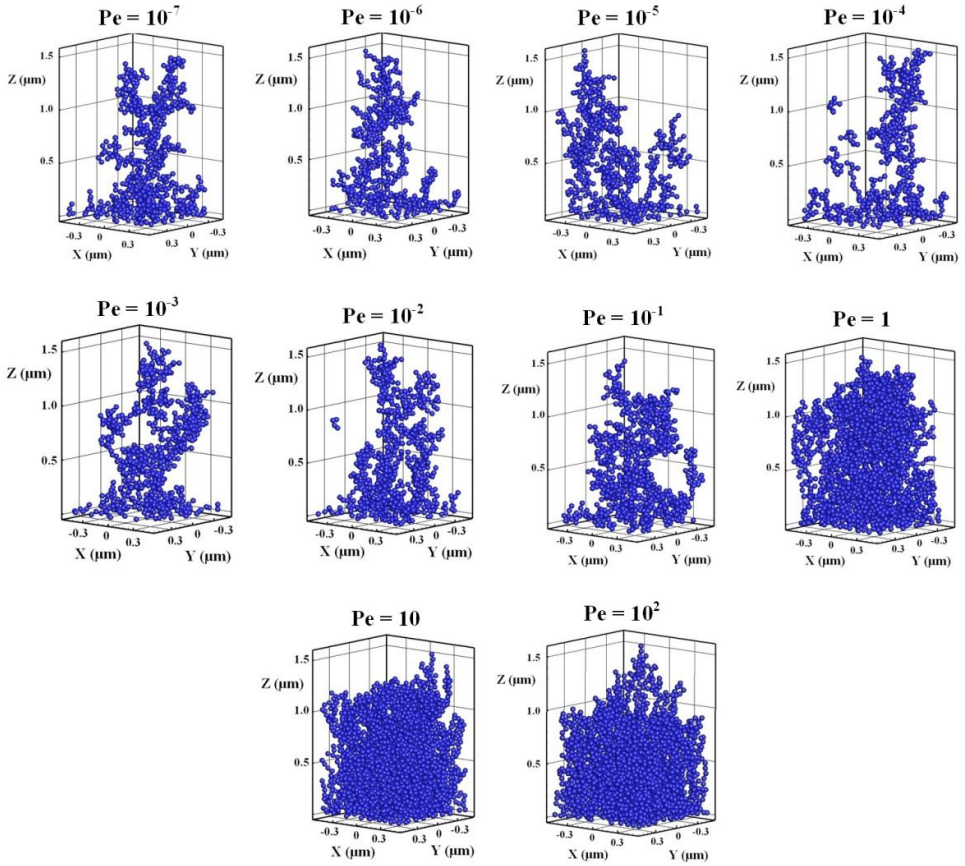

Figure 4: Visualization of the nanoparticle films (50 nm particle size) at a thickness of 1.5 µm as a function of the Pe number.

Conclusions

Porous films made of nanoparticle deposition have recently found several applications as solar cells and sensitive gas sensors. In this research, the morphology and evolution of the deposited film structure were investigated by Langevin dynamics. The results showed that the highest porosity was obtained for low Pe numbers where particle transport was dominated by diffusion and the lowest porosity was at high Pe numbers (ballistic regime) where the translational velocity is dominant. By transition from diffusion to ballistic limit, the deposition mechanism of the nanoparticles changes from tree-like at lower Pe number to bush-like at higher ones. This different deposition mechanism changes the number of deposited particles required to reach at the same thickness. The number of deposited particles at 1.5 μm thickness increases from 747 to 2590 for Pe increasing from 10^{-7} to 100.

REFERENCES

[1] Poizot, P., Laruelle, S., Grugeon, S., Dupont, L. and Tarascon, J-M., "Nano-sized transition-metal oxides as negative-electrode materials for lithium-ion batteries," Nature 407, 496-499 (2000).

[2] Tricoli, A., Wallerand, A.S. and Righettoni, M., "Highly porous TiO_2 films for dye sensitized solar cells," J. Mater. Chem., 22, 14254 (2012).

[3] Maheshwari, V. and Saraf, R.F., "High-resolution thin-film device to sense texture by touch," Science 312, 1501-4 (2006).

[4] Thyboa, S., Jensenb, S., Johansenc, J., Johannessenc, T., Hansenb, O., and Quaadea, U.J., "Flame spray deposition of porous catalysts on surfaces and in microsystems," J. Catal. 223, 271 (2004).

[5] Fleischer, M., Simon, E., Rumpel, E., Ulmer, H., Harbeck, M., Wandel, M., Fietzek, C., Weimar, U. and Meixner, H., "Detection of volatile compounds correlated to human diseases through breath analysis with chemical sensors," Sens. Actuator B: Chem. 83, 245–249 (2002).

[6] G. Eranna, B. C. Joshi, D. P. Runthala, R. P. Gupta, "Oxide Materials for Development of Integrated Gas Sensors-A Comprehensive Review," Crit. Rev. Solid State Mater. Sci. 29, 111 (2004).

[7] Korotcenkov, G., "Gas response control through structural and chemical modification of metal oxide films: state of the art and approaches," Sens. Actuators B 107, 209 (2005).

[8] Sberveglieri, G., Faglia, G., Groppelli, S. and Nelli, P., in Proc. 6th Int. Conf. Solid-State Sens. Actuators (Transducers91), San Fran-cisco (USA), p. 165 (1991).

[9] Kennedy, M. K., Kruis, F. E., Fissan, H., Mehta, B. R., Stappert, S. and Dumpich, G., "Tailored nanoparticle films from monosized tin oxide nanocrystals: Particle synthesis, film formation, and size-dependent gas-sensing properties," J. Appl. Phys.93, 551 (2003).

[10] Barsan, N. and Weimar, U., "Conduction model of metal oxide gas sensors," J. Electroceram. 7, 143 (2001).

[11] Madler, L., Lall, A.A. and Friedlander, S.K., "One-step aerosol synthesis of nanoparticle agglomerate films: simulation of film porosity and thickness," Nanotechnology 17, 4783–4795 (2006).

[12] Madler, L., Roessler, A., Pratsinis, S.E., Sahm, T., Gurlo, A., Barsan, N. and Weimar, U., "Direct formation of highly porous gas-sensing films by in situ thermophoretic deposition of flame-made Pt/SnO_2 nanoparticles,", Sensors Actuators B, 114283–95 (2006).

[13] Simpkins, P.G., Greenberg-Kosinski, S. and MacChesney, J.B., "Thermophoresis mass-transfer mechanism in modified chemical vapor-deposition," J. Appl. Phys., 505676–81 (1979).

[14] Kulkarni, P. and Biswas, P., "A Brownian dynamics simulation to predict morphology of nanoparticle deposits in the presence of interparticle interactions," Aerosol Sci. Technol., 38541–54 (2004).

[15] Rodríguez-Pérez, D., Castillo, J.L. and Antoranz, J.C., "Relationship between particle deposit characteristics and the mechanism of particle arrival," J. physical review E72, 021403 (2005).